Extremely High-order Optimized Multioperators-based Schemes and Their Applications to Flow Instabilities and Sound Radiation

Andrei Tolstykh, Michael Lipavskii, Dmitrii Shirobokov, and Eugenii Chigerev

Dorodnicyn Computing Center, Federal Research Center "Computer Science and Control" of Russian Academy of Sciences, Russian Federation,
tol@ccas.ru,
Moscow, Russian Federation

Abstract. Multioperators-base schemes up to 32nd-order for fluid dynamics calculations are described. Their parallel implementation is outlined. The results of applications of their versions to instability and sound radiation problems are presented. The extension to strongly discontinuous solutions is briefly outlined.

Keywords: Multioperators-based schemes· Euler and Navier-Stokes equations· Parallel methodology· Instabiity and sound radiation· Jets· Discontinuous solutions

1 Introduction

The multioperators technique proposed in [1] is a way to construct arbitrary high-order numerical analysis formulas and, in particular, arbitrary high-order approximations to fluid dynamics equations. High orders are obtained via increasing numbers of *basis operators* with fixed stencils rather than by enlarging stencils or polynomial orders (that is, by increasing numbers of *basis functions*). The basis operators are generated by one-parameter families of compact approximations $L_h(c)$ to a target linear operator L and the resulting multioperators look like

$$L_M(c_1, c_2, \ldots, c_M) = \sum_{i=1}^{M} \gamma_i L_h(c_i) \tag{1}$$

where $c_1, c_2, \ldots, c_M$ are the input values of parameter c. The c_i values uniquely define the γ_i coefficients making approximation orders proportional to either M or $2M$. Considering them as free parameters, one can control the multioperators properties.

As follows from Eq. (1), calculations of the multioperators actions on known grid functions involve performing similar arithmetic operations for each parameter c_i. Thus multioperators-based numerical analysis formulae can be calculated

in a parallel manner. That property can be used also for constructing parallel algorithms for Computational Fluid Dynamics (CFD) applications.

Several types of multioperators were investigated and used in CFD algorithms, the main tasks being 2D and 3D Navier-Stokes problems for compressible gas flows . Some theoretical topics can be fond in particular in [2]. Various types of high-order multioperators-based numerical analysis formulae are described in [3]. In [5], a family of extremely high order multioperators based on two-point compact approximations to derivatives is presented. The resulting conservative linear and non-linear schemes can be used for smooth and discontinuous solutions. The complete theory of multioperators can be found in [4].

Below a brief overview of the latest both theoretical and numerical results is presented.

2 Schemes outlines

Using the uniform mesh $\omega_h : (x_j = jh, j = 0, \pm1, \pm2, \ldots), \quad h = const$, the multioperators family under consideration can be created in the following way. First, the two-point operators depending on parameter c are introduced in the form

$$R_l(c) = I + c\Delta_-, \quad R_r(c) = I - c\Delta_+ \tag{2}$$

where Δ_- and Δ_+ are the two-point left and right differences. Then the upwind-downwind pair for approximating the first derivatives with the truncation orders $O(h)$ are defined by

$$L_l(c) = \frac{1}{h} R_l(c)^{-1}\Delta_-, \quad L_r(c) = \frac{1}{h} R_r(c)^{-1}\Delta_+. \tag{3}$$

Assuming the Hilbert space of bounded grid functions with the inner product defined by the summation over grid points, they have the same skew-symmetric component and the self-adjoint components with opposite signs. It follows from the Eq. (3) that very simple two-diagonal inversions of the operators from (2) are needed to calculate the actions of operators L_l and L_r on known grid functions.

Now the skew-symmetric second order operator $L_h(c)$ in Eq.(1) is defined as $L_h(c) = (L_l(c) + L_r(c))/2$. Fixing M values $c_1, c_2, \ldots c_M$ and solving the linear system for γ_i coefficients, one obtains the skew-symmetric multioperator $L_M(c_1, c_2, \ldots, c_M)$ providing the approximation order $O(h^{2M})$ for derivatives of sufficiently smooth functions. Additionally, we construct the self-adjoint multioperator defined by

$$D_{M_1}(\bar{c}_1, \bar{c}_2, \ldots, \bar{c}_{M_1}) = \sum_{i=1}^{M_1} \bar{\gamma}_i L_1(\bar{c}_i), \quad \sum_{i=1}^{M_1} \bar{\gamma}_i = 1 \tag{4}$$

where $L_1 = L_l(c) - L_r(c))$ and M_1 is possibly differs from M; in the following it is however assumed that $M_1 = M$. For fixed values $\bar{c}_i, i = 1, 2, \ldots M_1$, the $\bar{\gamma}_i$ coefficients can be obtained to give $D_{M_1}[u]_j = O(h^{2M_1-1})$ where $[u]_h$ is a

sufficiently smooth function projected into mesh ω_h. To simplify the multioperators investigations, we always suppose that the parameters values are linearly distributed inside the intervals $[c_{min}, c_{max}]$ and $[\bar{c}_{min}, \bar{c}_{max}]$. In this way, the multioperators become two-parameter dependent.

In the case of model equation

$$\frac{\partial u}{\partial t} + \frac{\partial f(u)}{\partial x} = 0, \tag{5}$$

the semi-discretized scheme in the index-free form reads

$$\frac{\partial u}{\partial t} + L_M(c_{min}, c_{max}) f(u) + C\, D_M(\bar{c}_{min}, \bar{c}_{max}) u = 0, \quad C \geq 0. \tag{6}$$

Setting $f(u) = au$, $a = const$ and using the Fourier transform, the c_{min}, c_{max} values can be used to control the spectral properties. The $\bar{c}_{min}, \bar{c}_{max}$ values were considered as admissible if $D_M(\bar{c}_{min}, \bar{c}_{max}) \geq 0$. Then scheme (6) is stable in the L_2 norm as a scheme with a non-negative operator. The term with D_M is the high-order dissipation mechanism which can be used to damp possible spurious oscillations.

Scheme Eq. (6) can be readily extended to multidimensional cases by constructing the multioperators for each spatial coordinate independently. Consider, for example, K-dimensional conservation laws in the case of vector valued functions $\mathbf{u}$, $\mathbf{f}_k(\mathbf{u})$, $k = 2, 3$

$$\frac{\partial \mathbf{u}}{\partial t} + \sum_{k=1}^{K} \frac{\partial \mathbf{f}_k(\mathbf{u})}{\partial x_k} = 0. \tag{7}$$

Using uniform meshes ω_k and the above defined operators for each spatial coordinate x_k, the k^{th} multioperator looks as

$$L_M^{(k)}(c_{min}, c_{max}) = \sum_{i=1}^{M} \gamma_i L_0^{(k)}(c_i), \quad D_M^{(k)}(\bar{c}_{min}^{(k)}, \bar{c}_{max}^{(k)}) = \sum_{i=1}^{M_k} \bar{\gamma}_i^{(k)} L_1^{(k)}(\bar{c}_i) \tag{8}$$

where the basis operators $L_0^{(k)}$ and $L_1^{(k)}$ are the L_0 and L_1 ones corresponding to the ω_k mesh. It is suggested in Eq (8) that dissipative multioperators $D_{M_k}(\bar{c}_{min}^{(k)}, \bar{c}_{max}^{(k)})$ can be different for different coordinates x_k while the main skew-symmetric multioperators are defined uniquely for each coordinate.

The semi-discretized scheme for Eq.(7) now reads

$$\frac{\partial \mathbf{u}}{\partial t} + \sum_{k=1}^{K} L_M^{(k)} \mathbf{f}_k(\mathbf{u}) + \sum_{k=1}^{K} C_k\, D_M^{(k)} \mathbf{u} = 0, \quad C_k \geq 0. \tag{9}$$

Considering the Hilbert space of vector-valued functions, one can prove that the scheme under some assumptions concerning the Jacobian matrices is stable in the frozen coefficients case. It can be readily cast in the flux form.

The Euler equations may be viewed as a particular case of the governing equations Eq. (7). In the case of the Navier-Stokes equations, various approximations to the viscous terms can be added to Eq. (9). For example, they can be compact or multioperators ones.

2.1 High resolution during long-time integration

Returning to the scalar 1D case, the dependence of the multioperators on two parameters allows one to control their spectral properties. The well accepted way to characterize the properties of approximations to convection terms is to consider the exact numerical solutions of the semi-discretized advection equation obtained from (5) by setting $f(u) = au$, $a = const$. In our case, the exact solution of Eq.(6) with $u(0, x) = exp(ikx)$ reads

$$u_j = \exp(-Cdt/h)\exp(ik(hj - a_*t)), \quad a_* = a\hat{L}_M(\alpha, c_{min}, c_{max})/\alpha,$$
$$d = h\hat{D}_M(\alpha, \bar{c}_{min}, \bar{c}_{max}).$$

The difference between the numerical phase velocity a_* and the exact one a can be viewed as the phase errors while function $d(\alpha) > 0$ is responsible for the harmonics damping. It can be viewed as a measure of amplitude errors. Clearly, even small phase errors can produce large solution errors for large time values t. Using the free parameters c_{min}, c_{max}, the optimizing procedure minimizing the phase errors for as large intervals of the dimensionless wave numbers $\alpha = kh$ as possible can be readily carried out. This was done for the 16th,20th,32nd and 36th - order schemes.

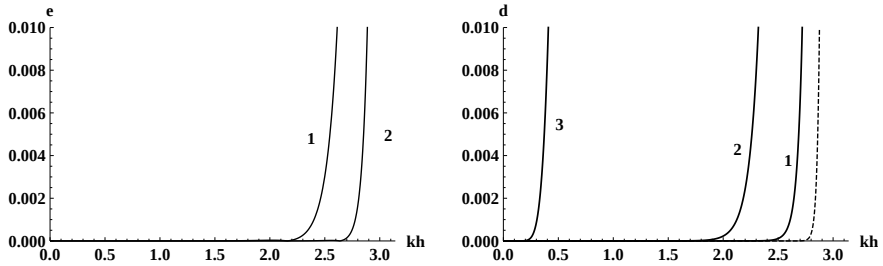

(a) (b)

Fig.1. a: Phase errors vs. wave numbers; 1:16th-order,2: 32nd-order; b: Dissipation exponent vs. wave numbers; 1,2,3: 15th-order, various choice of $\bar{c}_{min}, \bar{c}_{max}$.

Fig.1a shows the phase errors $e(\alpha) = |a_*/a - 1|$ for the 16th- and the 32th -order multioperators. They correspond to the near-optimal values of c_{min} and c_{max} obtained by calculating the functions for selected points in the two-dimensional space of the parameters. As follows from the Figure, the range of dimensionless wave numbers $[0, \alpha_*]$ for which the phase errors are small is noticeably greater for the 32th-order multioperator than that for the 16th-order one. Moreover, the "small" values of the errors shown by both curves in the Figure can differ by orders of magnitude indicating the advantages of the 32th-order multioperator. As an illustration, Table 1 presents the phase errors e for the selected values of the dimensionless wave numbers.

Table 1. Phase errors e for the selected values of α.

α	1.5	2.0	2.2	2.5
16th order	1.70e-6	1.8e-5	1.7e-5	1.2e-3
32th order	4.9e-11	5.6e-8	5.3e-7	7.7e-6

The amplitude errors introduced by multioperator D_M are characterized by the dissipation exponent $d(\bar{c}_{min}, \bar{c}_{max})$. Their dependance on wave numbers are shown in Fig.1b for several parameter pairs. Curves1,2,3 correspond to the 15th-order multioperator. They look as cut-off filters of high wave numbers harmonics with various cut-off values. Choosing $\bar{c}_{min}, \bar{c}_{max}$, one can control the dissipation property of schemes. The dashed curve in Fig.4 is obtained for near maximum cut-of value of the 31st-order multioperator.

To estimate the ability of the the schemes to preserve high resolution during long-time integration, consider the benchmark problem [6] for the advection equation (5) with $f(u) = u$ and the initial condition

$$u(0, x) = [2 + \cos(\beta x)][\exp(-\ln 2\,(x/10)^2)].$$

The task is to calculate the numerical solutions at $t = 400$ and $t = 800$ for $\beta = 1.7$ using mesh size $h = 1$. Parameter β is equal to our parameter α for that mesh size. Deviations from the exact solution (which is the travelling wave package containing very short waves harmonics defined by the initial condition) allow one to estimate the resolution, dispersion and the dissipation properties of the tested schemes. The problem can be solved exactly using the Fourier transform. The obtained solutions for a given spatial linear operator can provide the upper estimates of the maximum values of the time units t_{max} for which deviations from the exact solutions are less than some tolerance ε. Fig.2 shows functions $t_{max}(\beta)$ for $\varepsilon = 0.1$ and several spatial operators(defined by the second-order central difference, the fourth-order compact Collatz approximation and the 16th and 36th-order multioperators). As seen, large phase errors for high wave numbers can prevent reasonable description of harmonics advection during large time intervals in the case of non-optimized relatively low-order schemes. Clearly, filtering and time stepping devices can decrease t_{max} values.

The calculations were carried out for the higher than required wave number ($\beta = 2.1$ instead of $\beta = 1.7$) using the 32nd-order multioperator. Both numerical and exact solutions are presented in Fig.3 at $t = 15000$ (markers and solid lines correspond to the numerical and the exact solutions)showing very good dispersion-preserving property of the optimized multioperator.

3 Parallel implementation

The important multioperators property is the possibility to calculate their actions on known grid functions by parallel calculations of the actions of their basis

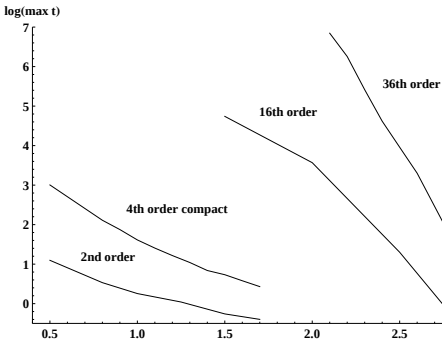

Fig.2 Maximum time units for which solution errors are less than 10 percent.

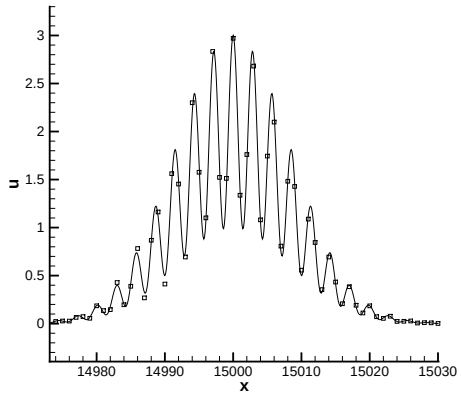

Fig.3. Numerical solution at $t = 15000$ obtained with 32th-order multioperator .

operators. It can be used for example in the framework of MPI when performing calculations with multicore PC. In the case of massively parallel system for solving 3D CFD problems, it can be combined with domain decomposition approaches exploiting considerable amount of left and right sweeps. Their number for a line along which the left and right sweeps are carried out can be estimated as $K = 5M$ where M is the number of parameters defining the multioperator. For example, one has $K = 20$ for the 16th-order scheme. Each sweep consists of calculating a current value with known previous one differing only in the parameters values and the functions which derivatives are approximated. Considering for example, the general form of the left sweep for a grid value v_i with $i = 1, 2, \ldots, N$, the process looks as

$$v_i = a(c_j)v_{i-1} + b(c_j)f_i,\ j = 1, 2, \ldots, M \tag{10}$$

where f_i is a known grid function. Thus it is possible to use m processors by partitioning the interval $i \in [0, N]$ into m equal parts with transferring the value calculated by the k-th processor to the $(k+1)$-th one, $k = 1, 2, \ldots m-1$. Using the idea, the calculations for one-line left sweeps with m processors can be schematically outlined in the form of Table 1 where "sweep k" means the calculations according Eq. 10.

As seen, some processors are idle at some stages. However the duration of $(K + m)$ stages is $(K + m)\tau$ where τ is time needed for each part of the decomposed space interval. Neglecting the data transfer expenses and comparing with the time $Km\tau$ in the case of a single processor , one obtains the speed up s equal to $Km/(K+m)$. It increase approximately linear if $m << K$ giving, for example, $s = 8$ for $K = 40$, $m = 10$. The above "one-line" idea applied to the 3D Euler or Navier-Stokes equations looks as follows. Supposing for the sake of argument that there are m^3 processors and a $N_x \times N_y \times N_z$ mesh, the computational domain is partitioned into $m \times m \times m$ cubes with m cubes in each spatial

Table 2. Organizing parallel calculations for K sweeps

processors	1	2	3	4	...	m
stage 1	sweep 1					
stage 2	sweep 2	sweep 1				
stage 3	sweep 3	sweep 2	sweep1			
...	...	...	...	...	...	
stage K	sweep K	sweep K-1	sweep K-2	...	...	sweep K-m+1
stage K +1		sweep K	sweep K-1	...	...	sweep K-m
...	...	...	...	...	...	
stage K+m						sweep K

directions (say, x,y and z ones). Considering for example the sweeps along x-coordinate, all processors are supposed to be involved in the calculations sweeps along N_yN_z/m^2 lines intersecting their $x = const$ faces of the cubes. Thus the time needed to calculate the x-derivatives in each grid point of the computational domain is $N_yN_z(K + m)\tau/m^2$. The same operation performed by a single processor requires $N_yN_zm\tau$ time (in reality, it is $N_yN_zm\tau_1$, $\tau_1 < \tau$ due to the data transferring loses). It gives the "ideal" speed-up s_x for the calculations along the x-coordinate $s_x = Km^3/(K+m)$. One has $s_x \approx m^3$ if $K >> m$. Having in mind that the total number of the processors N_p is equal to m^3, one has $s_x \approx N_p$. Upon finishing the job for the x-coordinate, the same processors perform the calculations for the y-coordinate and finally for the z-coordinate thus preserving the "ideal" speed-up.

In Table 2, the calculation times for our 3D Euler calculations of jets instability with several number of the processors of the Lomonosov supercomputer of the Moscow State University are presented, the MPI programming being used. The mesh was $360 \times 100 \times 100$. The processors were distributed for three spatial coordinates as $m \times m \times m$ with m ranging from 2 to 10.

Table 3. Execution times per time step and acceleration

Number of processors	8	27	64	125	216	1000
Distributions	$2 \times 2 \times 2$	$3 \times 3 \times 3$	$4 \times 4 \times 4$	$5 \times 5 \times 5$	$6 \times 6 \times 6$	$10 \times 10 \times 10$
Time per step, sec	113	27.45	12.64	6.34	3.99	1.70
Acceleration	1	4.12	8.94	17.8	40.3	66.5

In the above Table, the acceleration is defined as the time decrease when comparing with the case of $m = 2$.

4 Numerical examples

4.1 Applications to jets instabilities

The constructed schemes fit neatly into computational aeroacoustic requirements. They allow to describe properly pressure pulsations which amplitudes are

about 10^{-6}-10^{-7} of mean pressure levels when solving the Euler or the Navier-Stokes equations, no linearization or introducing base flows being needed.

Calculations with 10th-order multioperators schemes were carried out for cold and hot axisymmetric jets using both Cartesian and cylindrical coordinates analytically transformed to condense grid points near shear layers. The boundary conditions at nozzles lips were posed either as the results of the nozzles flow calculations or using analytical expressions (as in [7]) providing various initial shear layers thicknesses. Instabilities resulting in the break down of the steady state of the jets with vortex rings formation and sound radiations were investigated using both axisymmetric and 3D forms of the governing equations. It was found that the axisymmetric formulation is incomplete due to the excitation of azimuthal modes appearing in the 3D calculations. The snapshots of the vorticity fields in both cases are shown in Fig.4 and Fig.5 with more regular structure of the vorticity in the axisymmetric case.

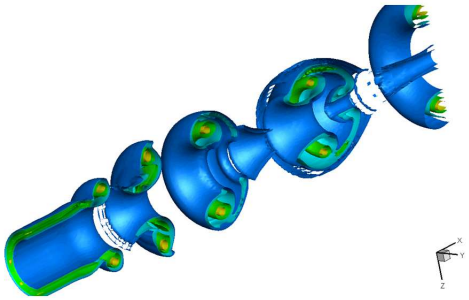

Fig.4 Snapshot of the vorticity field. Axisymmetric formulation

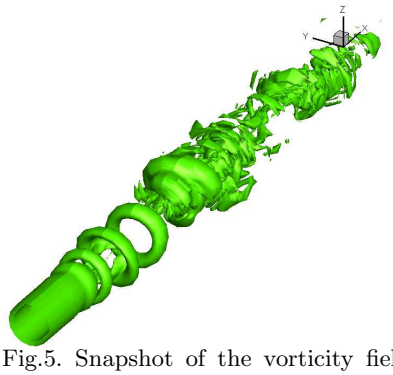

Fig.5. Snapshot of the vorticity field. 3D formulation

Fig.6 and Fig.7 shows the examples of the acoustic pressure spectra calculated for the microphones placed at points with polar coordinates $r = 20R, \theta$ where R is the initial jet radius, the origin being places at the center of the initial cross section of the jets. In the Figures, the curves differ in that they correspond to the boundary conditions at the nozzle lips specified in analytical forms (labelled as "synthetic",red lines) and obtained via flow calculations in the nozzle (green lines). The results of the calculations with the Cartesian grid are also shown in the Figures (blue lines).

The thicknesses of the shear layers at the jets boundaries were different in all presented cases causing different sound pressures levels seen in the figures. However the general form of the spectra looks very similar.

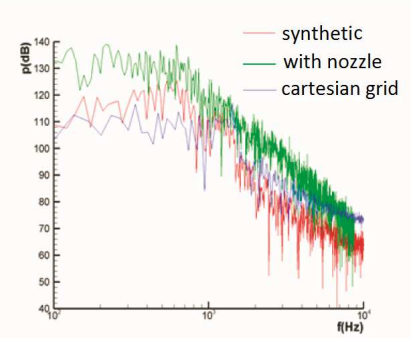

Fig.6. Spectra of acoustics pressures for 3D calculations; $r = 20R$, $\theta = 10^0$

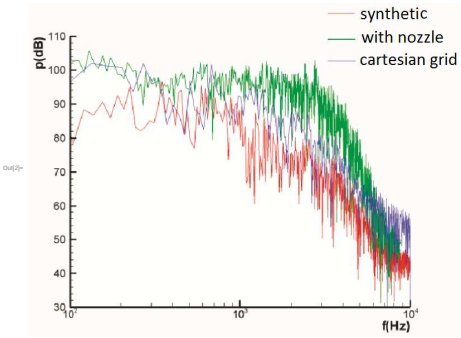

Fig.7. Spectra of acoustics pressures for 3D calculations; $r = 20R$, $\theta = 40^0$

Calculations with the multioperators schemes were carried out also for the 3D underexpanded jets in the case of narrow rectangular nozzles. They were aimed at the direct numerical simulation of the screech effect previously considered in the case of 2D nozzles [9]. The obtained acoustics fields generated by the unsteady behavior of the shock cells were found to correlate well with the 2D results. The calculated spectra with the main peaks close to the experimental ones looks very similar to those presented in [9].

4.2 Compact and multioperators schemes with Immersed Boundary Method (IBM)

High approximation orders of multioperators-based schemes is entirely due to exact solution smoothness allowing to get high-order terms in the corresponding Taylor expansion series. Thus smooth meshes are needed to provide peak performances of the schemes. Having in mind possible complexities when constructing smooth meshes for complex geometries, the IBM offers very good opportunity for using compact and multioperators-based schemes with the Cartesian coordinates when solving the Navier-Stokes equations. Skipping the extensive relevant literature, its earlier formulations were presented for example in [8].

In the present study, the direct forcing version of the IBM was applied to the compressible Navier-Stokes equations. The idea behind this is to get at least the second-order accurate solutions inside boundary layers at solid (in general moving) boundaries and highly accurate solutions away from them using non-adaptive to solid boundaries smooth meshes (for example, the Cartesian ones).

The 16th-order multioperators were used to approximate the inviscid terms of the compressible Navier-Stokes equations written for the Cartesian coordinates. Having in mind low-order representation of the boundary forcing terms, the viscous terms were discretized via the second-order centered differences.

In the present study, calculations for Mach number $M = 0.2$ were carried out using non-local high-order approximations (5th-order compact and 16h-order multioperators-based) with the sweeps along the Cartesian coordinate lines, the presence of the solid body being modelled by the forcing terms only. Bilinear or Radial Basis Functions (RBF) interpolants were used to define the values of the dependent variables at the near-boundary points outside or inside the cylinder. Several meshes were used to verify the mesh-convergence and good agreements with existing experimental and numerical data for low Reynolds data.

In the near-resolved case $Re \leq .400$, the calculation clearly showed the Von Karman vortex streets behind t5he cylinder. Fig.8 presents the vorticity field for $Re = 400$ while Fig.9 shows the acoustic spectrum for that case.

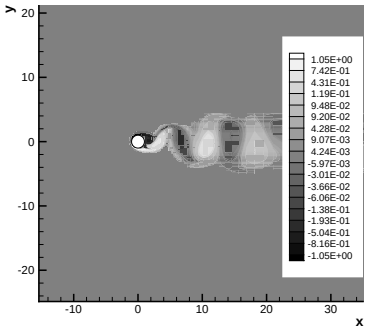

Fig. 8 $Re = 400$: snapshot of the vorticity field.

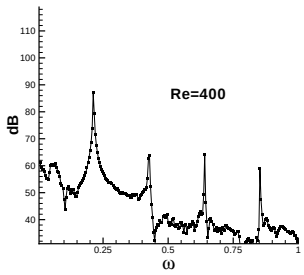

Fig. 9. $Re = 400$: acoustic spectrum.

Fig. 10 shows good agreement between calculated Strouhal numbers and various numerical and experimental data. The acoustic spectrum in the case of underresolved boundary layer ($Re = 10^8$) is displayed in Fig. 11.

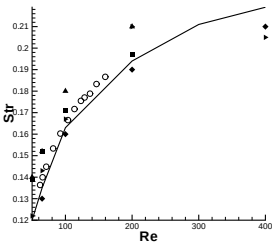

Fig. 10. Strouhal number vs. Reynolds number.

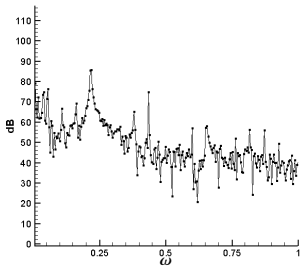

Fig. 11. $Re = 10^8$: acoustic spectrum.

4.3 Using the 32nd- and 16th-order multioperators in the case of strong discontinuities.

The conservative property of the multioperators-based schemes with dissipation mechanisms allows one to use them in the case of relatively small Mach numbers supersonic flows. In those cases, high-order dissipation mechanisms can be sufficient to suppress spurious oscillations. An example is the results of numerical simulations of underexpanded jets at $M \leq 1.5$ [9] with clear pictures of the screech waves. However monotonization devices are needed in the high Mach number cases. Following the well known ways, non-linear schemes can be constructed. The main aim in the multioperators context is to obtain numerical solutions combining reasonable shocks and contacts descriptions and high accuracy and high resolution away from the discontinuities. In [5], the hybrid schemes with the 16th- and 32th-order multioperators are tested against 1D problems (discontinuous solutions of the Burgers equation, extremal Riemann problems). Extending testing calculations, the double Mach reflection problem [10] was considered. Fig.12 shows the calculated density field resulting from a shock front hitting a ramp which is inclined by 30 degrees. The calculation were carried out using the 16th-order hybrid scheme from [5] and the setup described in [10] but with coarser mesh (the mesh sizes are $h_x = h_y = 1/60$).

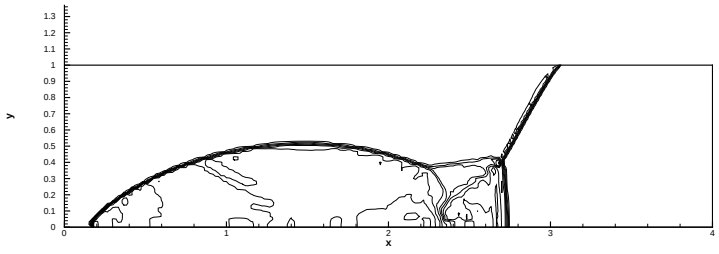

Fig.12. Double Mach reflection problem; density contours.

References

1. A.I.Tolstykh, Multioperator high-order compact upwind methods for CFD parallel calculations, in: D.R. Emerson et al. (Eds.) Parallel Computational Fluid Dynamics, Elsevier ,1998, pp. 383-390.
2. A.I. Tolstykh. Development of arbitrary-order multioperators-based schemes for parallel calculations. 1. Higher-than-fifth order approximations to convection terms. J. Comput. Phys. 225 ,2007, 2333-2353
3. A.I.Tolstykh, On the use of multioperators in the construction of high-order grid approximations, Computational Mathematics and Mathematical Physics, 2016, Vol. 56, No. 6, pp. 932-946.

4. A.I.Tolstykh, High accuracy compact and multioperators approximations for partial differential equations. Nauka, Moscow, 2015
5. A.I. Tolstykh, On 16th and 32th order multioperators-based schemes for smooth and discontinuous fluid dynamics solutions,Commun. Comput. Phys., 22,(1977), 572-598.
6. C.K.W.Tam, Problem 1-aliasing, In: Fourth Computational Aeroacoustics (CAA) Workshop on benchmark problems, NASA/CP-2004-2159, 2004
7. L. Lesshafft, P. Huerre,P. Sagaut, Frequency selection in globally unstable round jets, Phys. Fluids, 19 (2007) 054108-1–054108-10.
8. *Ming-Chih Lai, C.S. Peskin.* An Immersed Boundary Method with Formal Second-Order Accuracy and Reduced Numerical Viscosity// Journal of Computational Physics,160 (2000),705-719
9. A.I. Tolstykh, D.A. Shirobokov, Fast calculations of screech using highly accurate multioperators-based schemes, J. Appl. Acoustics. 74 (2013) 102-109.
10. P. Woodward, P. Colella. The numerical simulation of two-dimensional fluid flow with strong shocks. J. Comput. Phys., 54 (1984),115-173